

# SANDIA REPORT

SAND2015-8155

Unlimited Release

Printed September 2015

## High Accuracy Transistor Compact Model Calibrations

Charles E. Hembree, Alan Mar, Perry J. Robertson

Prepared by

Sandia National Laboratories

Albuquerque, New Mexico 87185 and Livermore, California 94550

Sandia National Laboratories is a multi-program laboratory managed and operated by Sandia Corporation, a wholly owned subsidiary of Lockheed Martin Corporation, for the U.S. Department of Energy's National Nuclear Security Administration under contract DE-AC04-94AL85000.

Approved for public release; further dissemination unlimited.



**Sandia National Laboratories**

Issued by Sandia National Laboratories, operated for the United States Department of Energy by Sandia Corporation.

**NOTICE:** This report was prepared as an account of work sponsored by an agency of the United States Government. Neither the United States Government, nor any agency thereof, nor any of their employees, nor any of their contractors, subcontractors, or their employees, make any warranty, express or implied, or assume any legal liability or responsibility for the accuracy, completeness, or usefulness of any information, apparatus, product, or process disclosed, or represent that its use would not infringe privately owned rights. Reference herein to any specific commercial product, process, or service by trade name, trademark, manufacturer, or otherwise, does not necessarily constitute or imply its endorsement, recommendation, or favoring by the United States Government, any agency thereof, or any of their contractors or subcontractors. The views and opinions expressed herein do not necessarily state or reflect those of the United States Government, any agency thereof, or any of their contractors.

Printed in the United States of America. This report has been reproduced directly from the best available copy.

Available to DOE and DOE contractors from  
U.S. Department of Energy  
Office of Scientific and Technical Information  
P.O. Box 62  
Oak Ridge, TN 37831

Telephone: (865) 576-8401  
Facsimile: (865) 576-5728  
E-Mail: [reports@adonis.osti.gov](mailto:reports@adonis.osti.gov)  
Online ordering: <http://www.osti.gov/bridge>

Available to the public from  
U.S. Department of Commerce  
National Technical Information Service  
5285 Port Royal Rd  
Springfield, VA 22161

Telephone: (800) 553-6847  
Facsimile: (703) 605-6900  
E-Mail: [orders@ntis.fedworld.gov](mailto:orders@ntis.fedworld.gov)  
Online ordering: <http://www.ntis.gov/help/ordermethods.asp?loc=7-4-0#online>



SAND2015-8155  
Unlimited Release  
Printed September 2015

# High Accuracy Transistor Compact Model Calibrations

Charles E. Hembree  
Radiation Effects Research 1344  
cehembr@sandia.gov

Alan E. Mar  
Microwave and Sensor Engineering 5443  
amar@sandia.gov

Perry J. Robertson  
RF and Opto Microsystems 1751  
pjrober@sandia.gov

Sandia National Laboratories  
PO Box 5800  
Albuquerque, NM 87185

## **Abstract**

Typically, transistors are modeled by the application of calibrated nominal and range models. These models consist of differing parameter values that describe the location and the upper and lower limits of a distribution of some transistor characteristic such as current capacity. Correspondingly, when using this approach, high degrees of accuracy of the transistor models are not expected since the set of models is a surrogate for a statistical description of the devices. The use of these types of models describes expected performances considering the extremes of process or transistor deviations.

In contrast, circuits that have very stringent accuracy requirements require modeling techniques with higher accuracy. Since these accurate models have low error in transistor descriptions, these models can be used to describe part to part variations as well as an accurate description of a single circuit instance. Thus, models that meet these stipulations also enable the calculation of quantification of margins with respect to a functional threshold and uncertainties in these margins.

Given this need, new model high accuracy calibration techniques for bipolar junction transistors have been developed and are described in this report.

# Acknowledgments

This report would not be possible without these contributions.

Charles Morrow

The organization and formatting of the experimental measured data used in the investigations in this report is the work of Charles Morrow. In addition, over the course of the work, there was ongoing collaboration with Charles Morrow concerning the makeup of the measured data and the technical specifications of how it was measured.

Don King

The generation of the data for several hundred transistors in this study was orchestrated by Don King. Don also explored numerous technical aspects of making novel measurements of advanced semiconductor devices.



# Contents

<b>Preface</b>	<b>11</b>
<b>Nomenclature</b>	<b>12</b>
<b>1 Introduction to High Accuracy Requirements in Modeling</b>	<b>13</b>
1.1 Examples of High Accuracy Simulation Scenarios . . . . .	14
1.1.1 High Precision Voltage Regulation Circuits . . . . .	14
1.1.2 Modeling Part to Part Variations . . . . .	15
<b>2 Transistor Models</b>	<b>17</b>
2.1 Gummel Poon model description . . . . .	17
2.2 VBIC model description . . . . .	18
<b>3 Modeling and Measuring the Transistors with Data Transformations Applied</b>	<b>21</b>
3.1 Challenges Inherent to Modeling Transistors . . . . .	21
3.2 Description of Data Transformation . . . . .	22
3.3 Comparison of Collector Current Data and Models with Transformation . . . . .	23
3.4 Comparison of Base Current Data and Models with Transformation . . . . .	26
3.5 Dominant Parameters of the VBIC Model . . . . .	30
<b>4 Automating the Optimization Process</b>	<b>35</b>
4.1 Overview of the Optimization Process . . . . .	35
4.2 Managing the Optimization Process . . . . .	36
4.3 Data Preparation and Process Sequencing . . . . .	36

4.3.1	Applying the Metric Calculation to the Transformed Data .....	37
4.3.2	Graphical Method of Comparison .....	37
4.3.3	Using a Circuit Simulator with an Optimization Routine .....	37
4.3.4	Combining Optimization Methods .....	38
4.4	Plotting Representation of the Process .....	38
4.4.1	Temperature Dependence of Final Optimization .....	40
<b>5</b>	<b>Summary and Conclusions</b>	<b>43</b>
	<b>References</b>	<b>44</b>
	<b>Appendix</b>	
<b>A</b>	<b>VBIC Model Parameters</b>	<b>47</b>

# List of Figures

3.1	Simulated collector (blue line) and base currents (red line) in amps as a function of applied $V_{BE}$ in volts. The base collector junction is held at 0 volts reverse bias in these simulations. ....	24
3.2	Simulated and measured collector current differences from a single exponential as a function of applied $V_{BE}$ . The simulation $\delta$ (blue line) compared to measured collector current $\delta$ (red dots). The base collector junction is held at 0 volts reverse bias in these measurements and simulations. ....	25
3.3	Simulated collector current $\delta$ as a function of applied $V_{BE}$ (blue line) compared to measured collector current (red dots). The base collector junction is held at 4 volts reverse bias in these measurements and simulations. ....	26
3.4	Simulated base current $\delta$ as a function of applied $V_{BE}$ (blue line) compared to measured base current $\delta$ (red dots). The base collector junction is held at 0 volts reverse bias in these measurements and simulations. ....	27
3.5	Simulated base current $\delta$ as a function of applied $V_{BE}$ (blue line) compared to measured base current $\delta$ (red dots). The base collector junction is held at 4 volts reverse bias in these measurements and simulations. ....	28
3.6	Simulated collector currents in amps (blue lines) as a function of applied $V_{CE}$ for several values of base currents compared to measured collector currents in amps (red dots). ....	29
3.7	Reproduction of the plots in figures 3.2 and 3.4 with select parameters effects on particular parts of the $\delta$ curves. Collector current $\delta$ s appear in the left hand plot and base current $\delta$ s appear in the right hand plot. The VBIC model parameters that are dominant in particular regions of the data are shown on the plots. ....	30
3.8	Reproduction of the plots in figures 3.3 and 3.5 with select parameters effects on particular parts of the $\delta$ curves. Collector current $\delta$ s appear in the left hand plot and base current $\delta$ s appear in the right hand plot. ....	32
3.9	Left hand plot shows the reverse Gummel curve of a transistor and the right hand plot is a reproduction of the forward output characteristic plot in figure 3.6. In the left hand plot the upper set of curves is the emitter current and the lower set is the base current. Currents in both plots are in amps. ....	33

4.1	A snapshot of the automated process that performs the precision calibration using the data transformation. The top row shows the starting $\delta$ s of the measured data and model for four different datasets and the bottom row shows the final $\delta$ s after optimization of model parameter values. . . . .	39
4.2	A plot of the $V_{BC}=0$ collector and base currents demonstrating the high accuracy of the extracted VBIC model in matching the calibration data. . . . .	40
4.3	Plots comparing collector and base currents at $V_{BC}=0$ to data taken from -40 to +90°C. . . . .	41

# Preface

This report describes a model calibration technique developed for the high precision modeling requirements of individual circuits in experimental systems of interest to Sandia National Laboratories (SNL). Some of these systems incorporate III-V heterojunction bipolar transistors (HBTs) to explore advantages to circuits with corresponding silicon transistors. Because of these inherent advantages and the smaller variation of transistors characteristics to begin with, these III-V HBT's can be used in circuits that have high precision outputs. Therefore, this work focuses on applying this modeling technique to III-V HBT transistors.

These techniques have been developed so that similar modeling efforts can be applied to design and qualification activities of systems incorporating circuits with high accuracy requirements.

# Nomenclature

**SNL** Sandia National Laboratories

**BJT** Bipolar Junction Transistor

**HBT** Heterojunction Bipolar Transistor

**PN Junction** Boundary in semiconductor material separating P doped region from N doped region

**NPN** N-type P type N type Transistor

**PNP** P type N type P type Transistor

**III-V** semiconductor material consisting of semiconductors from the 3rd and 5th columns in the periodic table

**Doping** Intentional impurities in semiconductor material to enhance conductivity

**Compact Model** model of a circuit element used in numerical circuit solver codes.

**Gummel-Poon model** Industry standard compact model of a BJT

**VBIC** Vertical Bipolar Intercompany model. Industry standard compact model of a BJT or HBT.

**model parameter** Component of a compact model used in mathematical relationships within the model.

**DC** Direct Current. Describes static or slowly varying with time operation of semiconductor device.

**AC** Alternating Current. Describes moderate to high frequency operation of a semiconductor device.

**UQ** Uncertainty Quantification. The identification and assigning of magnitudes to variations of model parameters to represent variations in measured characteristics.

# Chapter 1

## Introduction to High Accuracy Requirements in Modeling

There are generally two types of errors in compact models which describe semiconductor devices operating under static or near static conditions. The first type of errors consist of discontinuities or 'glitches' in model simulations of devices which are due to inadequate smoothing between different regimes of device operation. It is not unusual for a model to describe these regimes with different sets of equations that may include certain physical mechanisms for one regime and exclude these mechanisms in another regime. If the transition model description between each regime is incomplete or inaccurate, discontinuities can occur in some simulated device characteristic.

Another type of model error occurs when the model reproduces device data curve features without kinks or glitches but has offsets or differing slopes for the characteristic being modeled. These errors may be attributable to inaccurate calibrations of model parameters or to model form error so that a region of the device characteristic is poorly represented.

This report examines the errors associated with this second category of model inaccuracy and attempts to minimize this inaccuracy through techniques which enhance optimization of model parameters.

Of this second category of errors, it is not uncommon for extracted models to reproduce the behavior with errors that range from a few % up to  $\sim 20\%$  for some characteristics. The acceptability of these errors is dictated by the use of the device (perhaps it's operation is confined to the best fitting region) and the requirements for the accuracy. It is usual for the parameter extraction to be an iterative process so various fits might be experimentally assessed in order to obtain optimum performance from the model.

Some applications require unusual levels of accuracy across a broad range of device operation. In this case, the acceptable errors can be fractions of a % and the model must constrain this error sometimes over many decades of characteristic magnitude. As can be imagined in this case, some thought must be given to the construction of the metric which measures the error over such a large variation in magnitude. Assuming that the model is capable of this degree of accuracy, the calibration process must reflect this accuracy requirement and be able to distinguish between varying levels of fitting to data. In a closed commercial calibration tool, the control of the fit metric and the calibration process itself may be limited.

The majority of semiconductor implementations involve state of the art or near state of the art small CMOS transistors in digital applications. In these uses, the bulk of the concern with model accuracy involves timing analysis of circuit performance or noise contributions to circuit behavior. Since the present work concerns devices operating in low frequency regimes, it has not been

applied to these situations. The techniques in this work should be extensible to model parameters relevant to these effects however. At present, the focus of these techniques has been on model parameters important in analog applications.

By experimenting with calibration procedures using custom software, It has been found that attention to the metric and the process is key to obtaining the lowest error fits possible with a given model. This report will describe this process of experimentation with a particular model, the VBIC (Vertical Bipolar InterCompany) model, which describes operation of modern bipolar transistor devices. Chapter 2 describes this model.

## **1.1 Examples of High Accuracy Simulation Scenarios**

There are potentially many scenarios in modeling circuits or subcircuits where high precision model fidelity could be required. Two examples are described here but other cases range from modeling to support design for manufacturing (DFM) to specific circuit requirements.

### **1.1.1 High Precision Voltage Regulation Circuits**

The need for stable and fixed voltage references has been long standing in the electronics industry. Internal standard voltages are used in systems where some quantity can be represented by voltage or charge and needs to be measured precisely. Conceptually, this is related to using some unit measurement to count a quantity. An example of this type of circuit is a Brokaw circuit [1] [2] [3] which is a type of stabilized band gap voltage circuit. The inherent high precision of this circuit is derived and thus the motivation for precision modeling is described in [4].

Essentially, band gap circuits work by forcing two transistors or semiconductor devices to conduct an equal amount of current. Resistors or other devices are used in conjunction with these conducting transistors to monitor the amount of current flowing through the transistors. Departures from equal currents in these ancillary devices can thus be expressed as a voltage difference and this voltage difference is used as an input to an operational amplifier. This op-amp is used to determine the controlling voltage to the conducting transistors and is configured with feedback to drive the controlling voltage to a determined value corresponding to specific equal currents through the transistors.

It is not unexpected that this value of controlling voltage and the magnitude of the equal currents depends on device characteristics and predicting this voltage or currents requires highly accurate models of these characteristics. These types of circuits therefore require much care in modeling and simulation.

## 1.1.2 Modeling Part to Part Variations

The abstract notes that a typical approach to transistor modeling is to create representative models that describe and bound a distribution of transistor characteristics. These 'high', nominal, and 'low' models are adequate for roughly describing the behavior of an ensemble of transistors but are less useful for applications where descriptions of individual transistors are important. One such application is to distinguish, through models, variations between transistors. This might be important with circuit-level uncertainty quantification where even small differences in transistor characteristics can lead to significant effects in circuits containing these transistors. This is especially the case with analysis of intra-wafer variability where the transistors are likely to be very uniform and the accuracy of modeling must be sufficiently fine-grained to resolve device-to-device variability.

These scenarios require a different modeling approach for a group of transistors where individual transistors are modeled to high degrees of accuracy ( $<1\%$  error). A statistical description of the devices is realized with this method by obtaining distribution information for individual model parameters directly from the resulting ensemble of models. This type of approach can be useful in simulating responses in a particular circuit to variations such as those due to processing and wafer-to-wafer variability.

Knowledge of how the parameters vary between devices enables analysis of circuit effects so that more information about the distribution of circuit behaviors can be obtained. A concrete example scenario where this approach is useful is one where a simulated circuit functionality undergoes a 'phase change' (such as turning on or off) due to variation of even a single model parameter. Models that simply bound the range of parameters do not yield information concerning the onset of this phase change. In the case where this phase change delineates the operational envelop of a circuit, modeling with this degree of precision is essential.



# Chapter 2

## Transistor Models

The Vertical Bipolar InterCompany (VBIC) model is a successor model to earlier generations of bipolar junction transistor models such as the Gummel-Poon model. To succinctly review the VBIC model, the Gummel-Poon model will be briefly described and the VBIC model will be compared and contrasted.

### 2.1 Gummel Poon model description

The Gummel-Poon model of a bipolar junction transistor (BJT) is a charge control model [5] which distinguishes it from the Ebers-Moll model upon which it is based. Whereas the Ebers-Moll model starts its description of terminal currents with a *Linking Currents* description of charge flow between device regions, the Gummel-Poon model considers the additional currents and effects from stored charge in the base. Usually these currents are of second order but are useful in describing phenomena such as the Early effect or high level injection into the base.

The typical implementation of the Gummel-Poon model into a circuit simulator such as *SPICE* (Simulation Program with Integrated Circuit Emphasis) uses 41 parameters to describe the behavior of a transistor. These 41 parameters are distributed over the forward and reverse operating modes of the transistor as well as the DC and AC modeling of device behavior so it is clear that approximations are inherent in the model and descriptions of some physical phenomena are eliminated from the model. An example is that the main base current is derived from the collector current through the gain parameter instead of being calculated from independent parameters. This precludes including an effect such as additional base current due to a reversal of current at the base-collector junction caused by Quasi-Saturation.

The Gummel-Poon model does include, however, non ideal base currents and contains parameters to allow a description of base current components originating from recombination currents in either the base-emitter or base-collector regions. It also includes phenomena important to high speed applications such as the increase in base transit time by carriers due to the base push-out into the collector at high currents (Kirk effect). Due to the inclusion of these important effects, the Gummel-Poon model has been the de-facto standard for modeling bipolar transistor for many years.

## 2.2 VBIC model description

The VBIC model builds upon the Gummel-Poon model and adds capabilities [6] [8]. This comes at a cost which is complexity and more parameters to be calibrated from data. The VBIC model has 101 parameters and as an example, the additional parameters allow for independent calculation of base and collector currents as opposed to the linked calculation in the Gummel-Poon model.

An important capability in the VBIC model and not in the Gummel-Poon model is the ability to calculate device self heating. This effect is important for advanced semiconductor and III-V devices because of the methods of constructing some III-V devices. In an isoplanar semiconductor process where high speed silicon double polysilicon BJTs or SiGe HBTs can be fabricated, the effects of self heating are less pronounced due to the material surrounding each transistor. The devices are built into the bulk semiconductor which can carry away excess heat. In a MESA HBT process, each layer of the device is built by deposition upon a substrate and the upper layers may not be surrounded by material. Thus, these layers have less conductive heat dissipation and therefore may experience wide temperature variations due to heat build-up from operation.

The self-heating model included in the overall VBIC Device Model is relatively simple. Self-heating is implemented by providing a separate device terminal, DT, which is connected to a current source whose value is proportional to the calculated power dissipation of the device. Internally a thermal resistor RTH is connected from the DT node to ground whose value has units of degrees Celsius per Watt (C/W). A capacitor CTH is connected in parallel providing a temperature time constant of  $1/(RTH*CTH)$ . The voltage at the node DT is then the rise in temperature of the device above the nominal temperature. The temperature of the device is given by the sum of the simulation temperature (TNOM) and the temperature rise V(DT).

A couple of points are worth mentioning here. The internal thermal network can be disabled by setting  $RTH=0$ . An external network can be connected to the DT node to provide a more sophisticated and accurate model of the temperature rise with respect to the device power dissipation. In GaAs HBT devices, the simulation temperature can have a dramatic effect on the base and collector currents, and vice versa. Although Section 4.4.1 discusses some work with temperature modeling in general, further discussion of this topic is beyond the scope of the current report.

Other differences from the Gummel-Poon model are:

- Improved Early effect modeling
- Quasi Saturation modeling
- Avalanche multiplication in collector junction modeling
- Electrothermal or self-heating modeling
- Parasitic substrate transistor modeling
- Modulation of collector resistance
- Parasitic capacitances of base emitter overlap in double polysilicon bipolar junction transistors

As can be surmised from many items in this list, the VBIC model is oriented towards modeling physical phenomena found in more modern and thus smaller bipolar junction transistor devices.



# Chapter 3

## Modeling and Measuring the Transistors with Data Transformations Applied

### 3.1 Challenges Inherent to Modeling Transistors

As suggested in Chapter 2 the challenge of comparing model fits to data is multifold for active semiconductor devices. Transistors can be operated in a forward active, reverse active, or a saturated state. Gummel curves and output characteristics are measured in each of the active states. Resistances and capacitances are measured for each of the terminals. All of these IV and electrical characteristics in each of these states must be described by the models incorporating appropriate parameter values.

Correlations between the parameters complicates the situation. For example, the forward Gummel data and the forward Output Characteristic data are correlated with device characteristics such as gain (which can be represented directly in the Gummel-Poon model and indirectly in the VBIC model). Adjustments to parameter values to fit more precisely the forward Gummel data may perturb the fit to the forward Output Characteristics. Often, pairs of parameters require adjustment in order to fit both IV characteristics. On the other hand, some groups of parameters are completely independent from other groups. Parameters such as terminal capacitances can be adjusted with no effect on DC characteristics such as Gummel Curves.

The task of optimizing parameters is made yet more formidable in the case of high accuracy requirements. Typically, model fit to data involves tradeoffs for better fit with some parts of the data and relaxed fits with other parts. This process is acceptable with wide error margins but is less desirable for lower error tolerances due to the high number of iterations required with the associated small perturbations to the trial fits.

In general the fitting of all model parameters of a complicated model like the VBIC model over several data sets has a dependence on sequence. This dependence includes the order of parameter perturbation to fit a particular set of data and also the order of the sets of data to fit. Thus, the process of parameter optimization influences the outcome.

Some of the difficulties in the process can be reduced by normalizing all of the deviations of model from data to a common magnitude scale and amplifying the deviations so that small perturbations of large numbers are not encountered. The normalization can be accomplished by use of a logarithmic scale for quantities that vary by many orders of magnitude. A Gummel curve is usually measured over 4 or 6 orders of current magnitude so this normalization is useful. The use of a logarithmic scale by itself, however addresses only part of the problem. On a log scale a model

fit which differs from data by 10% over many orders of magnitude can appear to match the data well even though an error of this magnitude may be unacceptable.

This error can be amplified by determining a common simple functional behavior to both the data and model fit and subtracting this behavior from both the model fit and the data. In both cases, the remainder or *residual* can be used for fitting. As will be seen, the fitting of the model residual to the data residual is more efficient than fitting the model to data. The computation of this residual or  $\delta$  is described in section 3.2. By amplifying this error and studying it in an optimization process, the best sequence for perturbing parameters for fitting can be more easily ascertained.

## 3.2 Description of Data Transformation

The collector current in a transistor operating in forward active mode is described in the VBIC model by [6]

$$I_C = \frac{I_{SF}}{q_b} \left( e^{\frac{V_{BE}}{(N_f V_{th})}} - 1 \right) + \frac{I_{SR}}{q_b} \left( e^{\frac{V_{BC}}{(N_r V_{th})}} - 1 \right) + I_{bci} \left( e^{\frac{V_{BC}}{(N_{ci} V_{th})}} - 1 \right) + I_{bcn} \left( e^{\frac{V_{BC}}{(N_{cn} V_{th})}} - 1 \right) + A_{v1} V_{BCmod} e^{-A_{v2} V_{BCmod}} \quad (3.1)$$

The exponential component of the first term describes the exponential forward active current. The remaining terms describe the contribution to the collector current originating at the base-collector junction. In particular, the last term describes the avalanche current that is caused by base-collector electric field induced breakdown.

Note that some Gummel-Poon corrections are included in this relationship by use of the normalized base charge  $q_b$ . This charge is computed as an integration of injected charge into the base from the emitter-base junction to the collector base junction. Bearing in mind that these junction locations are bias dependent, it can be seen that the normalized base charge can affect the collector current at high levels of injection. This effect causes the collector current to 'roll over' at high injection levels where the value of  $q_b$  changes rapidly with applied  $V_{BE}$ .

Not included in this description of the collector current components are the components of the base emitter currents which will be described in Section 3.4.

The forward active exponential current is the dominant term in the expression and can be approximated by:

$$I_C \simeq b * e^{m * V_{BE}} \quad (3.2)$$

where m and b are fitting parameters. Now, taking the natural log of these quantities and the difference between the forward active exponential current and it's approximation:

$$\ln(I_C) = \ln\left(\frac{I_S}{q_b}\right) + \frac{V_{BE}}{(N_f V_{th})} \quad (3.3)$$

$$\delta(V_{BE}) = \ln\left(\frac{I_S}{q_b}\right) + \frac{V_{BE}}{(N_f V_{th})} - \ln(b) - m * V_{BE} \quad (3.4)$$

This  $\delta$  should be fairly small in the region of  $V_{BE}$  of low current injection into the base and even into the region of  $V_{BE}$  corresponding to the onset of high current injection. Note that all of the terms involved with the base-collector junction should be constant for a fixed  $V_{BC}$ . This  $\delta$  is the quantity that is of most interest in high accuracy fitting. Plotting this versus  $V_{BE}$  gives a magnified view of the difference between the VBIC model and a pure exponential over a large range of  $V_{BE}$ s. The same quantity

$$\ln(b) + m * V_{BE} \quad (3.5)$$

can be subtracted from the log of measured data for a transistor to determine how well a single exponential represents the data. Combining the plots of the model and data deviations from an exponential gives a magnified view of how well the model fits the data.

### 3.3 Comparison of Collector Current Data and Models with Transformation

Figure 3.1 displays simulated Gummel curves for a transistor operating in forward active mode. The vertical axis demarcates current magnitudes in amps for both the collector current (blue) and the base current (red). The horizontal axis is the voltage of the applied forward voltage at the emitter-base junction ( $V_{BE}$ ). The collector current for this device is about 2 orders of magnitude higher than the base current so the gain of this transistor is of order 100. Equation 3.1 generated the collector current over it's entire range of  $V_{BE}$  values. The collector current in the region from  $V_{BE}=0.4$  to  $0.7$  volts is approximately linear on the vertical log scale, so the collector current in this region can be described with a single exponential term.

The collector current data and simulations in this region can thus be considered in isolation and an expression such as equation 3.2 can be fitted to this data by adjusting the values of  $m$  and  $b$ . Subtracting a fitted equation 3.2 from the collector current simulation leaves the quantity that is plotted in Figure 3.2 as a blue line. The same equation 3.2 has been subtracted from measured transistor data and the remainder is plotted in the same figure as red open circles. These quantities are the  $\delta$ s in equation 3.4. The units on the vertical axis are differences between logarithmic current magnitudes. These differences are quite small in this case since the model is adjusted to fit the data. Because of the operation of taking the log of the simulation and data, a difference between simulation and data at low  $V_{BE}$  can be compared directly to a difference between simulation and data at high  $V_{BE}$ . In this comparison, the fit of the model to data can be evaluated over different regimes of device operation.

The offset of the plotted  $\delta$ s from 0 signifies that the fit to both the simulation and data is off by a scalar amount. In the case of an optimal fit, the inverted parabola shape of the  $\delta$ s would be centered about 0 with approximately half with positive values and roughly half with negative

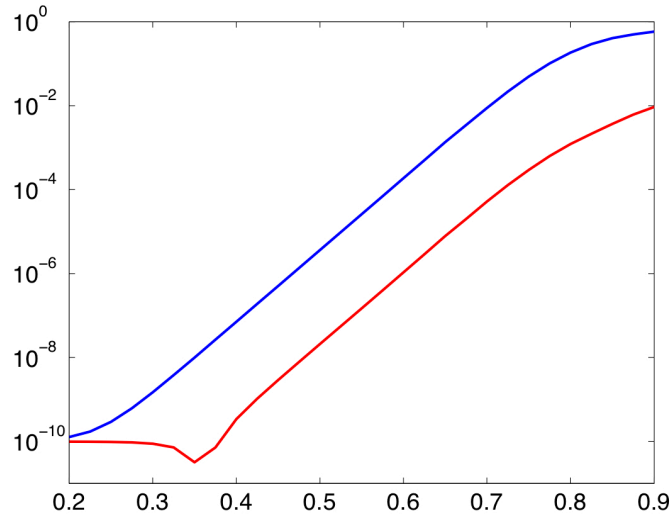


**Figure 3.1.** Simulated collector (blue line) and base currents (red line) in amps as a function of applied  $V_{BE}$  in volts. The base collector junction is held at 0 volts reverse bias in these simulations.

values.

The general shape of both the simulation and the data  $\delta$ s is parabolic but differences exist particularly in the  $V_{BE}$  range below 1 volts. As a reference, consider that a straight plot on this plot indicates that the corresponding collector current has an ideal exponential behavior. A horizontal straight line with 0 slope and passing through 0 will correspond to a collector current with ideal exponential behavior and with a perfect fitting exponential subtracted from it. With this in mind, consider the VBIC model and measured data  $\delta$ s separately.

The VBIC model does exhibit a pure exponential behavior for  $0.0 < V_{BE} < 1.05$  volts which is the left edge of the plot and below. The corresponding straight line (blue line) spans this range. The behavior change of the model at  $V_{BE}=1.1$  volts and above is dictated by the high injection behavior of  $q_b$  as described in section 3.2. The model describes a transistor with an exponential turn-on of the collector current with  $V_{BE}$  and a subsequent roll-off of the collector current at high current injection levels into the base.

The measured data is taken from a heterojunction bipolar transistor that is known to have a tunneling component to the collector current at low  $V_{BE}$  in addition to the exponential turn-on. Correspondingly, the data has a higher slope at low  $V_{BE}$  than the model and the data parabolically decreases as  $V_{BE}$  goes to 0. The measured data  $\delta$ s match the model in the mid to high  $V_{BE}$  range which indicates that the measured device experiences the transition from an collector current exponential turn on to high injection.

Therefore, the model closely matches the collector current data for the transition from the exponential region to the high injection region, but the model departs from the data in the low  $V_{BE}$  range. This comparison of the model to the data is conducted in a regime with these three transistor mechanisms, exponential turn on, tunneling current, and high injection. The characteristics of these mechanisms and whether they are present in both the model and data are easily seen in Figure 3.2 because of the applied transformation.

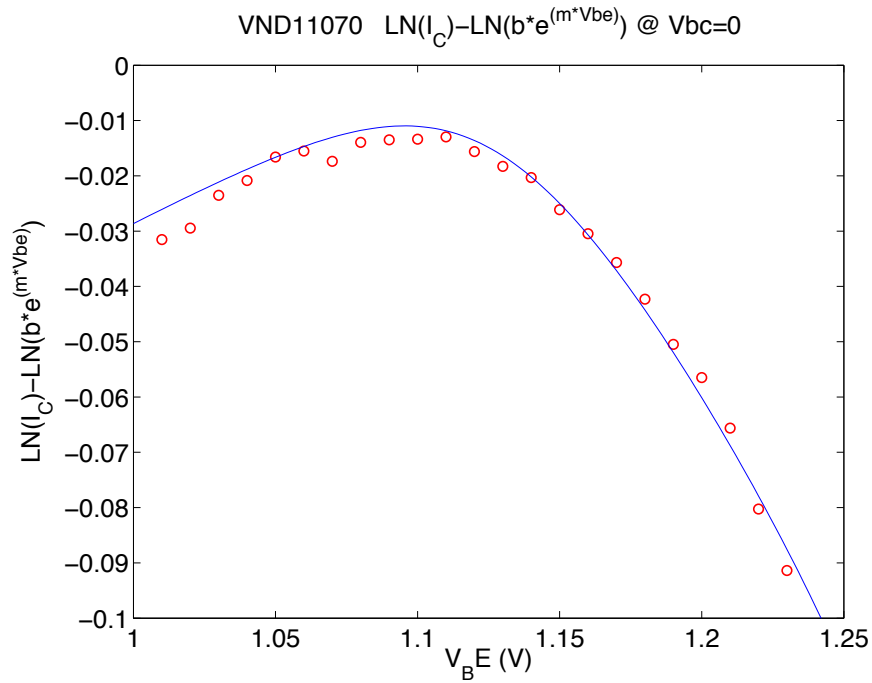


**Figure 3.2.** Simulated and measured collector current differences from a single exponential as a function of applied  $V_{BE}$ . The simulation  $\delta$  (blue line) compared to measured collector current  $\delta$  (red dots). The base collector junction is held at 0 volts reverse bias in these measurements and simulations.

More transistor effects are present in both the model and data when the base-collector voltage is increased. In the scenario above, the voltage across the base-collector junction was held at 0 volts which enforces a zero electric field across this junction. Applying a strong reverse bias field across this junction introduces new physical mechanisms which can be seen in both measured data and in simulations with the VBIC model.

Figure 3.3 shows the collector current  $\delta$ s as a function of  $V_{BE}$  with a base-collector voltage of 4 volts reverse bias. Again, the blue line is a VBIC model simulation with a subtracted single exponential and the red circles are measured data with the same exponential subtracted. The shape of the simulation and measured data has similarities to the shape in Figure 3.2. Both figures exhibit a peak of the collector current  $\delta$  around  $V_{BE}=1.1$  volts and in both cases the peak of the  $\delta$  is approximately -0.015. Thus the data and model are unchanged in the midpoint of the displayed  $V_{BE}$  range.

The base-collector reverse bias does make a difference at lower and higher  $V_{BE}$ s however. In both extremes, the collector current is higher than the single exponential behavior, particularly in the high injection roll-off. At low  $V_{BE}$ , the collector current is elevated due to leakage across the base-collector junction and the possible onset of avalanche breakdown current. Both of these current sources are a function of  $V_{BC}$  and are expected to be larger at a greater reverse bias. From an analysis perspective, it is difficult to separate the contributions of each of these sources to this

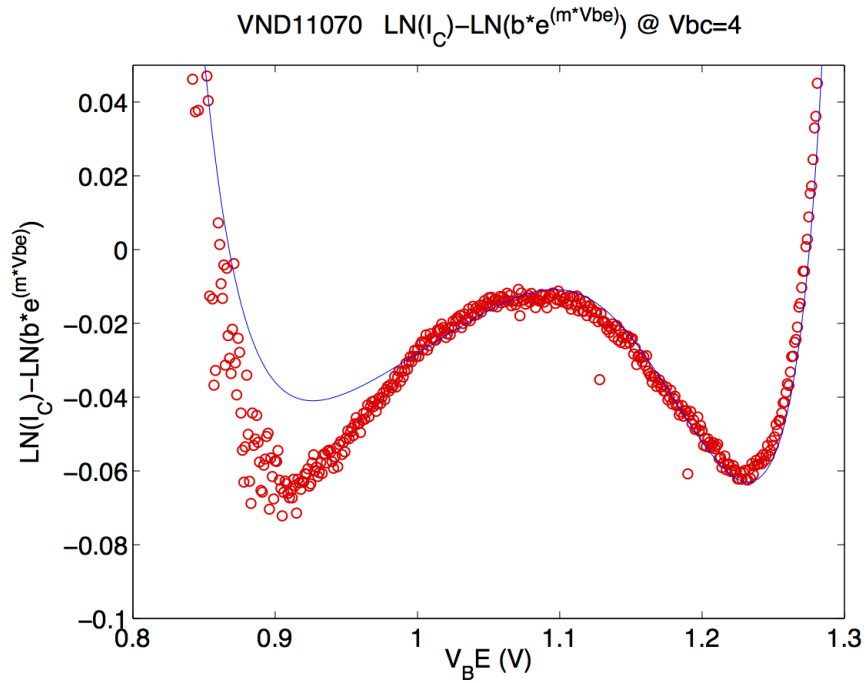


**Figure 3.3.** Simulated collector current  $\delta$  as a function of applied  $V_{BE}$  (blue line) compared to measured collector current (red dots). The base collector junction is held at 4 volts reverse bias in these measurements and simulations.

data without additional measurements. It is expected that the leakage component increases rapidly with temperature and repeating these measurements at additional temperatures may reflect this. Section 3.5 will discuss the modeling of these current sources in the VBIC model.

At high  $V_{BE}$ , the collector current is elevated due to the self heating in the device which results from the higher current densities. This phenomena occurs despite the transition to high injection operation and the resulting saturation of emitter current injected into the base. Even through the rate of increase of  $I_E$  falls off with  $V_{BE}$ , the heating of the devices from current crowding increases the total collector current.

### 3.4 Comparison of Base Current Data and Models with Transformation

The VBIC model describes the base current in a transistor as a sum of the base-emitter currents and the base-collector currents. (Equation 3.6). The base-emitter current is comprised of an ideal and non ideal component and a third base-emitter breakdown component. The base-collector components are the same components previously discussed with the collector current.

$$\begin{aligned}
I_B = & I_{bei} \left( e^{\frac{V_{BE}}{(N_{ei}V_{th})}} - 1 \right) + I_{ben} \left( e^{\frac{V_{BE}}{(N_{en}V_{th})}} - 1 \right) - \\
& - I_{bbe} \left( e^{\frac{V_{bbe} - V_{BE}}{(N_{bbe}V_{th})}} - 1 \right) + \\
& I_{bci} \left( e^{\frac{V_{BC}}{(N_{ci}V_{th})}} - 1 \right) + I_{bcn} \left( e^{\frac{V_{BC}}{(N_{cn}V_{th})}} - 1 \right) + \\
& A_{v1} V_{BCmod} e^{-A_{v2} V_{BCmod}}
\end{aligned} \tag{3.6}$$

In this case, there are two components of the total base current which can contribute to the exponential behaved base current as a function of  $V_{BE}$ . These are the ideal and non ideal components. Typically, the non-ideal component dominates at low  $V_{BE}$  and the ideal base current dominates at higher  $V_{BE}$ . It is therefore more difficult to approximate the base current with a single exponential term. Figure 3.4 plots the  $\delta$  of a base current simulation and measured data from a single exponential function that is fitted to the data and the simulation. In this Figure, the base-collector voltage is 0 volts while the base-emitter voltage is varied.

There are features in Figure 3.4 that make an interesting comparison to the analogous figure

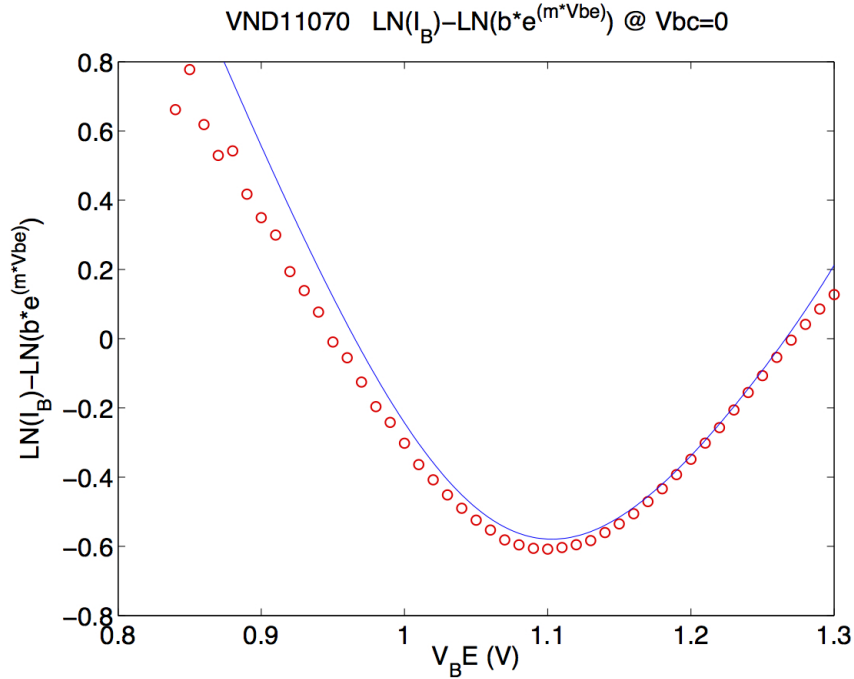


**Figure 3.4.** Simulated base current  $\delta$  as a function of applied  $V_{BE}$  (blue line) compared to measured base current  $\delta$  (red dots). The base collector junction is held at 0 volts reverse bias in these measurements and simulations.

for the collector current, Figure 3.2. The collector current departs from a pure exponential because

of the tunneling current having a stronger dependence on  $V_{BE}$  at low  $V_{BE}$  and the high injection roll-off at high  $V_{BE}$ . This departure is concave. In contrast, the departure of the base current from a pure exponential is convex and this is due partially to the two exponential makeup of the current. The non-ideal emission coefficient  $N_{en}$  is generally larger than the ideal emission coefficient  $N_{ei}$  and this leads to an elevated base current at low  $V_{BE}$  with respect to a single exponential fitted to the entire base current. Thus the  $V_{BE} < 1.1$  volt region in the plot matches the region where the non-ideal base current dominates and the region  $V_{BE} > 1.1$  volts corresponds to the ideal base current dominant region. The convex shape of the  $\delta$  in the plot is caused by the intersection of two regions where in each region, the base current can be approximated by a single exponential.

Another contrast from Figure 3.2 is that the magnitudes of the  $\delta$  in Figure 3.4 are more than an order of magnitude larger. Again, this is primarily due to the two exponential makeup of the base current whereas the collector current is describable by a single exponential with corrections. The single exponential is a cruder approximation in the base current case and the accompanying errors ( $\delta$ s) are larger.

The expectation for the base current is that the variation of the base-collector junction voltage will have a lesser effect upon the behavior of the base current  $\delta$  than in the case of the collector current. This is due to the shape being determined by the strong  $V_{BE}$  dependence of the two exponential currents rather than the addition of other current sources such as the base-collector leakage current. This is verified in Figure 3.5 which is seen to have very little change from Figure 3.4 despite the change in base-collector voltage to 4 volts.

The same fitted model displayed in the preceding figures has been used to generate a set of

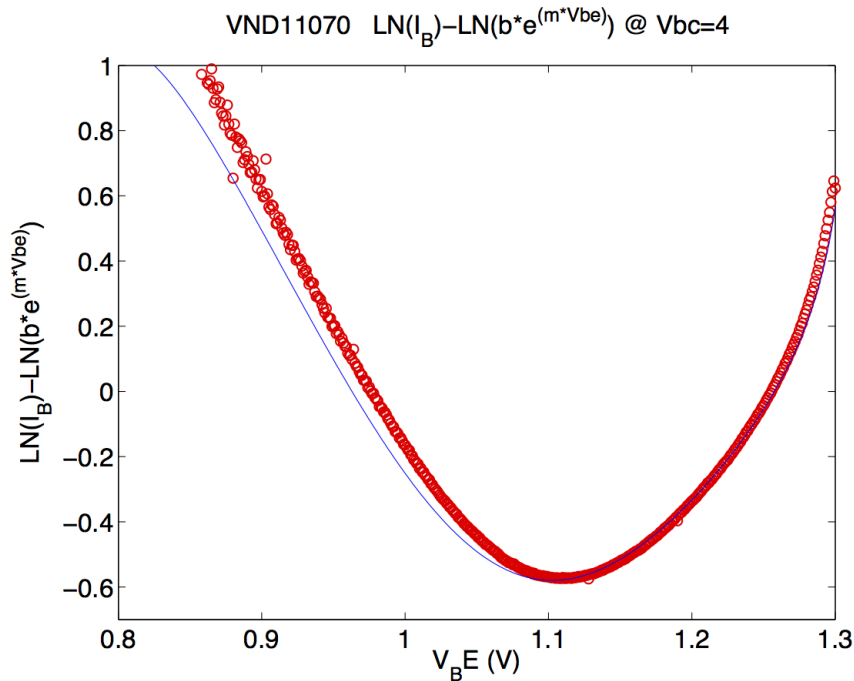


**Figure 3.5.** Simulated base current  $\delta$  as a function of applied  $V_{BE}$  (blue line) compared to measured base current  $\delta$  (red dots). The base collector junction is held at 4 volts reverse bias in these measurements and simulations.

forward output characteristic curves for the collector current. The generated curves are compared to measured data in the Figure 3.6. The output characteristic does not lend itself to a single characteristic behavior which can be subtracted from both the modeled characteristic or the measured data. Thus, Figure 3.6 does not have a counterpart figure with  $\delta s$  displayed. It is more difficult to assess the quality of the model fit to the data in this case.

These curves are generated by sweeping the collector voltage with respect to the emitter voltage while the base is stepped either in current or voltage. Each curve represents a discrete base voltage or current. Because of the collector voltage sweep, the collector current undergoes a polarity reversal and this occurs in Figure 3.6 at approximately 0.4 volts. The bias configuration at this polarity reversal (emitter-base junction forward biased, collector-base junction transitioning from forward bias to reverse bias) does not appear in any of the Gummel curves so fitting the model to the data in this region involves VBIC model parameters which weakly affect the modeling of the transistor in the forward Gummel curve operation.

As will be discussed in section 3.5, the  $V_{CE}$  value where the polarity of the simulated col-

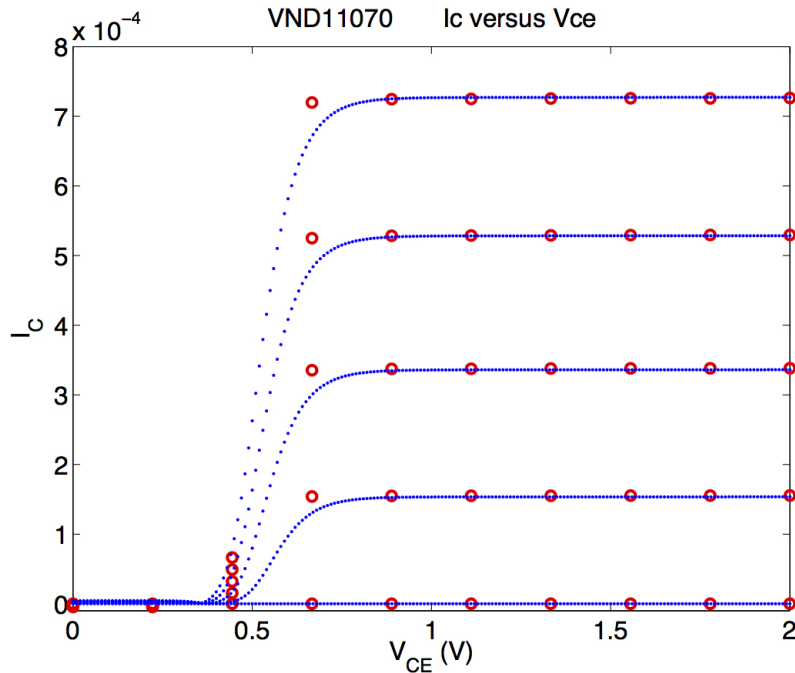


**Figure 3.6.** Simulated collector currents in amps (blue lines) as a function of applied  $V_{CE}$  for several values of base currents compared to measured collector currents in amps (red dots).

lector current reverses is dependent upon the VBIC model parameters which control the current leakage across the base-collector junction (saturation current) and the parameters which control the simulated onset of avalanche current across this junction.

### 3.5 Dominant Parameters of the VBIC Model

The preceding sections have described the application of the data transformation for bipolar transistor measured data and model generated data. The resulting  $\delta$ s from idealized behavior have been discussed along with correlating features of the  $\delta$  curves to physical mechanisms of transistor operation. This section examines the identification and optimization of relevant parameters to each curve so that the model curves have high fidelity with respect to the measured data in the transformed plots.

The first step in this process is to associate the appropriate VBIC model parameters with particular datasets and regimes of these datasets. For reference, all of the VBIC model parameters are listed and described in Appendix A. These tables group the parameters according to corresponding components of the model and this is the start of the process to associating parameters with particular datasets. Although there are 101 parameters in the model, approximately 25 parameters are varied to achieve the fits for the DC data that is considered in this work.

The first set of plots shown in Figure 3.7 are the  $V_{BC} = 0$  volts plots of the collector and base

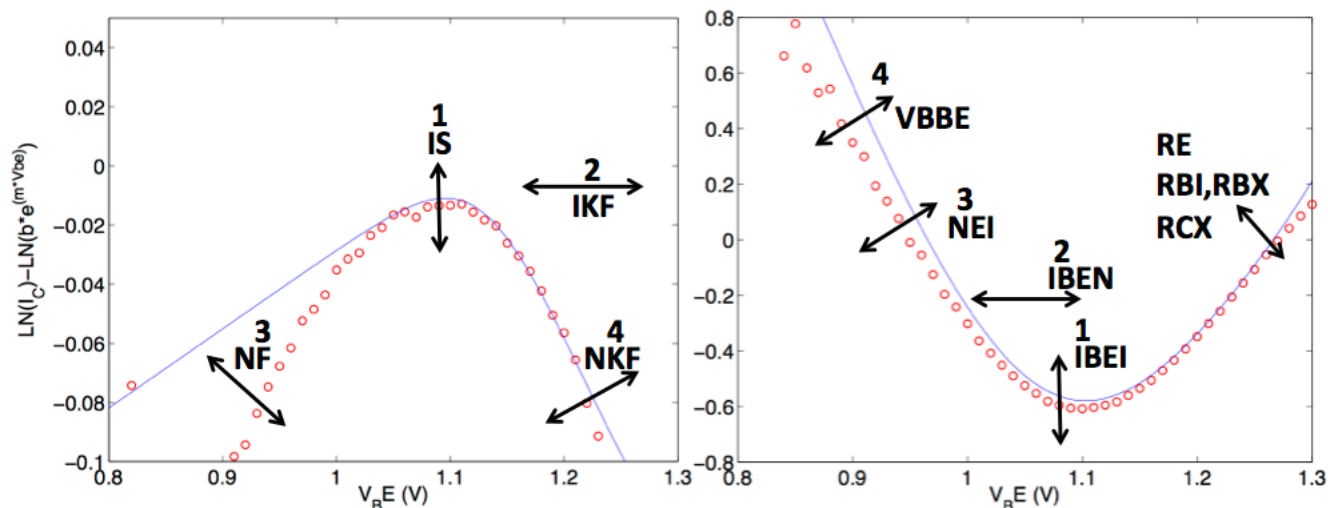


**Figure 3.7.** Reproduction of the plots in figures 3.2 and 3.4 with select parameters effects on particular parts of the  $\delta$  curves. Collector current  $\delta$ s appear in the left hand plot and base current  $\delta$ s appear in the right hand plot. The VBIC model parameters that are dominant in particular regions of the data are shown on the plots.

current  $\delta$ s with the transistor operated in the forward active mode. The data sets corresponding to these plots are the first groups of data to be fit in the optimization process. As expected therefore, the fitted parameters associated with this data are parameters which determine magnitude and slopes of the currents. The collector current  $\delta$ s are fit first followed by the base current  $\delta$ s. The order of the parameter fitting is given in each plot by the numbers associated with each parameter or group of parameters. Therefore, the first parameter to be fit in this stage of the process is IS and

the last group of parameters to be fit are the resistances RE, RBI, RBX, and RCX. As alluded to above, the first parameter in each plot is the magnitude determination parameter of the currents and thus the most fundamental (IS for collector current and IBEI for base current). It should be kept in mind, that these parameters are inputs to a model that determines currents but this optimization method is optimizing not the model fit to the currents but the fit of the differences (simulated and measured  $\delta s$ ) between the currents and some archetype function.

It is worth repeating some of the points raised in Section 3.2 about the correlation and independence of some of the parameters. As might be inferred from the separate plots, the parameters IS and IBEI determine the magnitude of separate curves and thus are independent of each other. However, for each curve some strong correlations exist. In the case of the collector current, IS and IKF are strongly correlated. In the base current case, IBEN and IBEI are strongly correlated. Although these two parameters correspond to non ideal and ideal base currents respectively, it is the ratio between the two which determines some of the strong fitting to the  $\delta s$  in Figure 3.7 right hand plot.

The left hand plot in Figure 3.7 also can be examined to illustrate a point in Section 3.3 about the correspondence of the model to the actual behavior of the device collector current at low values of  $V_{BE}$ . The left hand plot contains  $V_{BE}$  values as low as 0.8 volts. At these values, it is clear that the model  $\delta s$  (blue line) do not match the data  $\delta s$  (red circles) and thus the model is missing the tunneling current physics which the data exhibits. It is also clear that the model exhibits the straight line behavior in the region  $V_{BE} < 1.0$  volt that indicates that it is a single exponential in this region.

The second set of plots in Figure 3.8 are the collector and base current  $\delta s$  for the  $V_{BC}=4.0$  volts bias, again with the transistor operated in forward active mode. Most of the parameters optimized by working with the datasets corresponding to Figure 3.7 are optimized for these datasets as well. Thus most aspects of this data  $\delta s$  are fit well by the first model parameter set without additional optimization.

The additional transistor mechanisms in Figure 3.8 as compared to Figure 3.7 were discussed at the end of Section 3.3 and these additional features do require additional model parameters to fit. The leakage and avalanche onset (low  $V_{BE}$ ) at the base collector junction are determined by the parameters IBCI and AVC1, AVC2 respectively. The self heating part of the collector current model (high  $V_{BE}$ ) can be adjusted by RTH and the temperature coefficient of IS, XIS. The activation energy for IS, EA also influences the collector current. The base current at high  $V_{BE}$  is modeled by the activation energy of the emitter current, EAIE and the temperature coefficient of IBEI, XII.

Figure 3.9 shows the reverse Gummel plot of a transistor in the left hand plot and the forward output characteristic of the same transistor in the right hand plot. In both plots, the blue line represents the output of the VBIC model and the red circles represent the measured data for the transistor. Neither of these plots have been subjected to a data transformation as was performed with the forward gummel curves.

The reverse Gummel plot displays characteristics which indicate that it is potentially a good candidate for a data transformation. The emitter current displays a linear behavior on a log plot in the region  $V_{BC}=0.8$  to  $V_{BC}=1.3$  volts. An examination of equation 3.1 indicates that this behavior

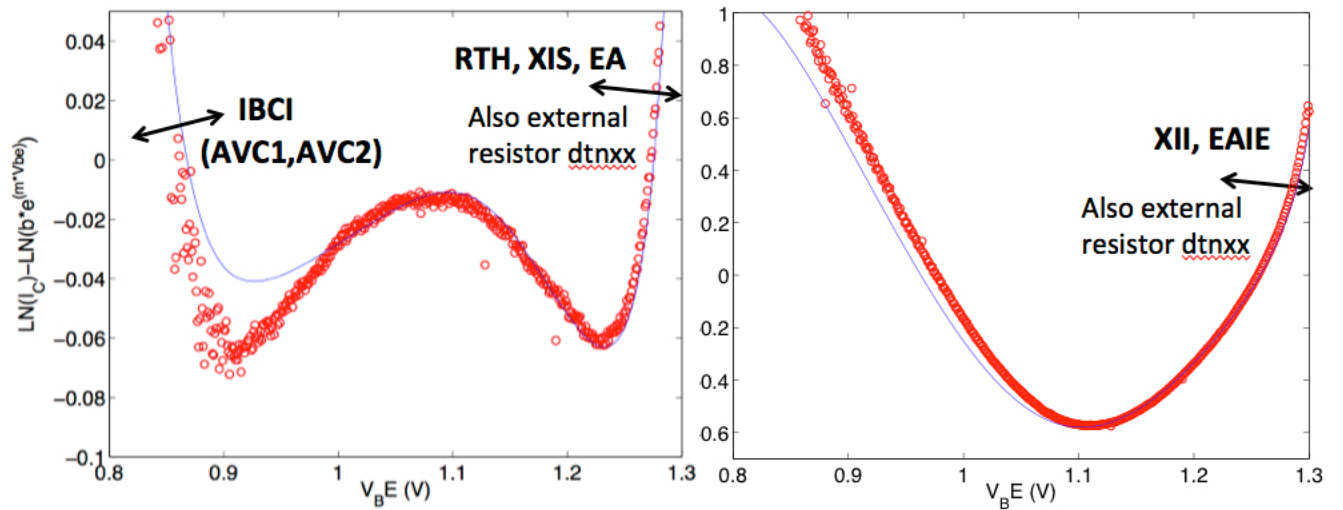


**Figure 3.8.** Reproduction of the plots in figures 3.3 and 3.5 with select parameters effects on particular parts of the  $\delta$  curves. Collector current  $\delta$ s appear in the left hand plot and base current  $\delta$ s appear in the right hand plot.

is due to the term

$$\frac{I_{SR}}{q_b} \left( e^{\frac{V_{BC}}{N_r V_{th}}} - 1 \right) \quad (3.7)$$

This term is descriptive of a quantity which could be subtracted from the model and the data to obtain a more detailed view of the ability of the model to fit the data. The base current in the same  $V_{BE}$  range also exhibits a linear behavior in the log plot which indicates that the data could be transformed in a similar fashion. In the present work, the desire for high accuracy model fits was limited to the forward operation of the device so this exercise was not explored for the reverse operation.

Despite the reduced need for accuracy for the reverse active operation of the transistor, several new parameters are explored in order to obtain fits with this data. Perhaps the most significant of these parameters are the emission coefficients associated with the ideal and non ideal saturation currents across the base collector junction, NCI and NCN. ISRR, IKR, and NR have not been previously defined but are analogous to the similar parameters for forward operation, (IS, IKF, NF). Together, these reverse parameters determine the fundamental magnitudes and slopes of the reverse currents.

The right hand plot in Figure 3.9 displays forward output characteristic curves for both model and measured experimental data. As mentioned earlier, a single data transformation was not explored for this data. However, a magnification of the vertical axis in a given region can show how well the model fits the data in the non-saturation region of  $V_{CE}$  which on this plot is the region where  $V_{CE} > 0.5$  volts. In this region, the collector current is essentially constant with respect to

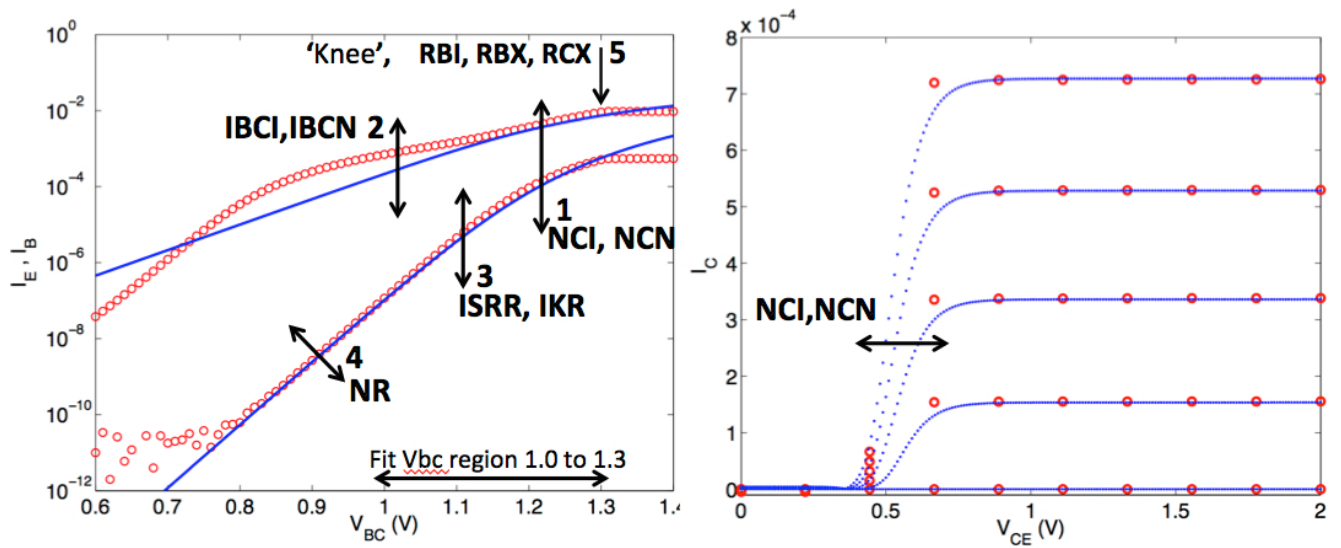


**Figure 3.9.** Left hand plot shows the reverse Gummel curve of a transistor and the right hand plot is a reproduction of the forward output characteristic plot in figure 3.6. In the left hand plot the upper set of curves is the emitter current and the lower set is the base current. Currents in both plots are in amps.

$V_{CE}$  (for a fixed  $V_{BE}$ ) for the magnitudes of  $V_{CE}$  shown in the plot. At higher values of  $V_{CE}$  other mechanisms such as avalanche multiplication lead to a non-constant  $I_C$ .

A fundamental feature of the data in the forward output characteristic is the value of  $V_{CE}$  where the polarity of the collector current reverses and the collector current increases to appreciable values at higher  $V_{CE}$ . This polarity reversal is partially set by the amount of leakage current across this junction and the magnitude of this leakage current is described by the parameter IBCI. The slope of the leakage current is set by the emission coefficients NCI and NCN. Since IBCI is usually set in the second set of parameter optimization associated with the forward active data taken at nonzero  $V_{BC}$ , the parameters NCI and NCN provide the adjustments necessary to match the collector current reversal in the forward output characteristic data.

Note that NCI and NCN can also adjust the magnitudes of the reverse gummel curves shown in the left hand plot of Figure 3.9 but other parameters (IBCI, IBCN, ISRR) also provide for this adjustment so freedom exists to adjust NCI and NCN in the forward output characteristic plot to obtain an optimal fit.

The order in which these dominant parameters have been discussed is the order in which these parameters should be optimized. Using the data transformation as part of the fitting process seems to reduce the need to iterate the entire process which is common in other approaches. Iterations in this approach take place in the fitting of specific groups of parameters and this is discussed in Chapter 4.

The parameters detailed in this section should provide the ability to optimally adjust the VBIC model to fit forward active Gummel data for DC operation including self heating. The DC forward saturated and reverse operation of the transistor can also be modeled with these parameters. AC

characteristics have not been included in this analysis but the techniques should be extendable.

# Chapter 4

## Automating the Optimization Process

As seen in the previous chapter, the data transformations enable high-accuracy parameter optimizations that lead to models capable of resolving device-to-device variability. Section 3.5 details the VBIC parameters used to obtain optimal model fits to measured transistor data that has been transformed with the technique of Section 3.2. The parameters are related to specific datasets (or subsets of datasets) and the parameters are typically optimized in pairs or groups of parameters. The section presents the parameter groups in the order in which the optimization flow occurs, thereby describing the high level process flow.

In order to obtain good statistics in applying such modeling to uncertainty quantification, it is desirable to apply this process to large numbers of devices with a consistent workflow. This motivates the development of an automated process to extract parameters for batches of devices without the need for manual intervention.

This chapter describes more details of the optimization process mechanics in an automated system applied to individual and groups of devices. These details include data preparation, comparisons to model calculations using specific metrics, and iteration techniques to obtain the best fit for a group of parameters.

### 4.1 Overview of the Optimization Process

The model calculations are performed with a SPICE simulator called Xyce, developed at SNL to study circuits and electrical systems [9]. The VBIC model is included in this simulator and it is exercised with trial parameter values during the optimization process. These trial values are generated by the optimization program Dakota (also SNL developed) [10] which is used to supply the circuit simulator with parameter values that heuristically reflect the optimization. For both measured data and simulated data, the transformation described in section 3.2 is applied and the goodness-of-fit between the transformed model  $\delta$ s and the transformed measured data  $\delta$ s is calculated. This goodness-of-fit drives the optimization process.

This key point, discussed previously, is worth repeating again. The goodness-of-fit is *not* generated for the untransformed model calculations and measured data. It is the application of the optimization to the fitting of the simulated  $\delta$  to the measured  $\delta$  that makes this process efficient and effective.

## 4.2 Managing the Optimization Process

This iterative optimization process for successive select subgroups of parameters is orchestrated by a coordinating script that calls the Dakota, Xyce, metric calculation, and plotting programs. Therefore, the addition (or subtraction) of fitting parameters in the process is managed at this level. Also determined at this level is the selection and number of transistors to model. The program has been applied to individual transistors or to groups as large as a few hundred. Preparing the measured data for this number of transistors requires automated routines for data formatting.

The optimization process begins with initial values and ranges of the parameters that are naturally coupled to a particular type of transistor under study. The initial model parameter values and ranges are dynamically computed from the data associated with a representative transistor. The values are obtained directly from the measured data through well established techniques. [7].

Several alternatives to the use of a representative parameter set exist. One such alternative is to use the finishing values of a preceding transistors's parameter optimization as starting values for the next transistor or group of transistors. In practice, the parameter extraction techniques are quick so using this successive optimization technique for groups of transistors is not strictly required. In fact, since the data extraction routines are fast, another alternative is to compute starting values for parameters directly from each transistors set of data. In this way, transistors of different types or different vintages of the same type can be optimized together, since the starting values of the parameters are customized for each transistor.

This initial parameter extraction can also input information to the algorithm that computes the  $\delta$ s of the measured data. Recall that a constant and the log of an approximation to the collector current data is subtracted from the data in equation 3.4 in order to compute the  $\delta$ . The slope of this approximation is used to determine the starting value of the emission coefficient of the collector current and the magnitude of the collector current approximation is used to determine the starting value for the saturation current  $I_S$ . Thus, computing these initial parameter values also computes the approximation.

## 4.3 Data Preparation and Process Sequencing

In the optimization process, measured test data  $\delta$ s are compared to model prediction  $\delta$ s with two methods. The first method is to quantitatively compare measured data  $\delta$ s to model generated data  $\delta$ s and to compute a metric which represents how well the model generated data  $\delta$ s represent the measured data  $\delta$ s. Typically this metric consists of a least squares estimate over some specified range of the data. The computation of this metric requires that both the measured data  $\delta$ s and the model generated data  $\delta$ s be read into a routine that performs the computation. This requirement determines the format of both types of data. As a side note, the least squares metric requires that the measured data and model generated data have the same values of the independent variable. This additional constraint on the data can be accomplished by an interpolation routine either within the metric computation routine or in the routine where the  $\delta$ s are calculated.

### 4.3.1 Applying the Metric Calculation to the Transformed Data

The two  $\delta$  vectors are subtracted point by point (independent variable) and the differences are squared, added together and averaged over the number of points in the vector. Again, this process is customarily applied to untransformed data but the widely varying differences in magnitude of untransformed data means that the larger datapoints can dominate the optimization process. The key to the current process is that the computed metric is of the transformed data where all of the  $\delta$ s are of similar magnitude and of order unity. These characteristics boosts the efficiency of the optimization routines within Dakota.

### 4.3.2 Graphical Method of Comparison

The second method of comparison is less formal and is simply to produce a plot of the measured and model generated data  $\delta$ s. Thus, the plot consists of the transformed data with greatly amplified errors and is used to visually verify the fidelity of the model to the data. Although no results from the plot are automatically fed back into the optimization process, plot information regarding model fidelity can be used by analysts to modify the optimization process as needed. This plotting also constrains the measured and model data  $\delta$ s to adhere to a specified format.

Obviously, the model generated and measured data must span the same range of the independent variable. A less obvious restriction on the data is that it must consists of enough data points to accurately represent the behavior of the transistor but not consist of a large number of data points that the simulation burden is time consuming.

### 4.3.3 Using a Circuit Simulator with an Optimization Routine

Measured transistor data is generated with a transistor and a simple circuit which typically consists of several power supplies to apply voltage and current viewing resistors. In order to model this test circuit setup, a transistor model such as the VBIC model is embedded in a representative circuit model of the test setup. Thus a circuit simulation tool with a required input file is used to generate the model data.

This circuit simulator is coupled to an optimization program that iteratively generates the trial values of the model parameters. The input file to the circuit simulator is a template file to describe the circuit topology along with the model specifications for the transistor. These model parameters are represented as dummy parameters in the template file which is populated with values as determined by Dakota. In practice, a circuit simulator file is built up by a script (for each iteration) which takes the circuit topology subsection and combines with a model specification with trial numerical values for the particular iteration.

### 4.3.4 Combining Optimization Methods

Dakota uses the metric to guide the computation of the next set of trial parameters. Since the metric represents the difference between the model generated  $\delta$ s and the measured  $\delta$ s, optimization proceeds by minimizing the metric. For systems with monotonic metric behavior, it is straightforward for Dakota to compute a minimizing direction in parameter space and generate sets of parameters corresponding to this direction.

For more general behavior however, it is best to use Dakota in a global search method to determine regions of parameter space where the metric exhibits global minimums. Once a region is determined, gradient based methods can then be used to search parameter space for the optimal parameter values. For these optimizations, a two-step hybrid parameter search method is therefore employed where the first step consists of a global search followed by the second step using a gradient based search.

## 4.4 Plotting Representation of the Process

The two-step optimization process is utilized for small groups of parameters for a particular dataset. A complete parameter set is optimized by utilizing a sequence of these two-step optimizations. This can be illustrated by a graphical representation of the process.

Figure 4.1 is a snapshot of the process as it proceeds through the optimization for a single transistor. The first plot generated is the upper left plot which represents the measured data and initial guess model-generated data  $\delta$ s for a  $V_{BC}=0$  set of collector current data. The plot below this plot represents various trial parameter sets and the corresponding  $\delta$ s. This plot is updated with each optimization iteration so the plot appearing here is again a snapshot out of many images. (In the Figure, it actually shows the results from the last set of model parameter values.) The bottom plot in the left hand column shows the  $\delta$ s corresponding to the best trial set of model parameters. For this  $V_{BC}=0$  collector data, the parameters shown in the left hand plot of Figure 3.7 (NF, IS, IKF, NKF) are the parameters varied to find the best fit. Note that this and subsequent optimizations focus on accuracy in the range of base-emitter voltage of greatest interest for circuit calculations, 0.9 to 1.3 Volts.

The next column shows the  $V_{BC}=0$  base current  $\delta$ s and the top plot shows the initial model parameter set guess for the same individual transistor. The middle plot in this column shows the results from the last of the permutations of the model parameter set (In this case, the parameters in the right hand plot of Figure 3.7 (IBEI, IBEN, NEI, VBBE, RE, RBI, RBX, RCX)). The bottom plot in the column shows the  $\delta$ s corresponding to the best fit set of parameters. Similarly, the next two columns are the  $V_{BC}=4$  collector and base current cases. Each column is generated from top to bottom and the columns are generated from left to right in the optimization process.

After the  $V_{BC}=4$  base current optimization in column four is completed, the reverse Gummel characteristic is matched using the parameters shown in the left hand plot of Figure 3.9. In order to utilize a single page of plots, the second row of the fourth column is replotted to display the real-time permutations and final results of this process.

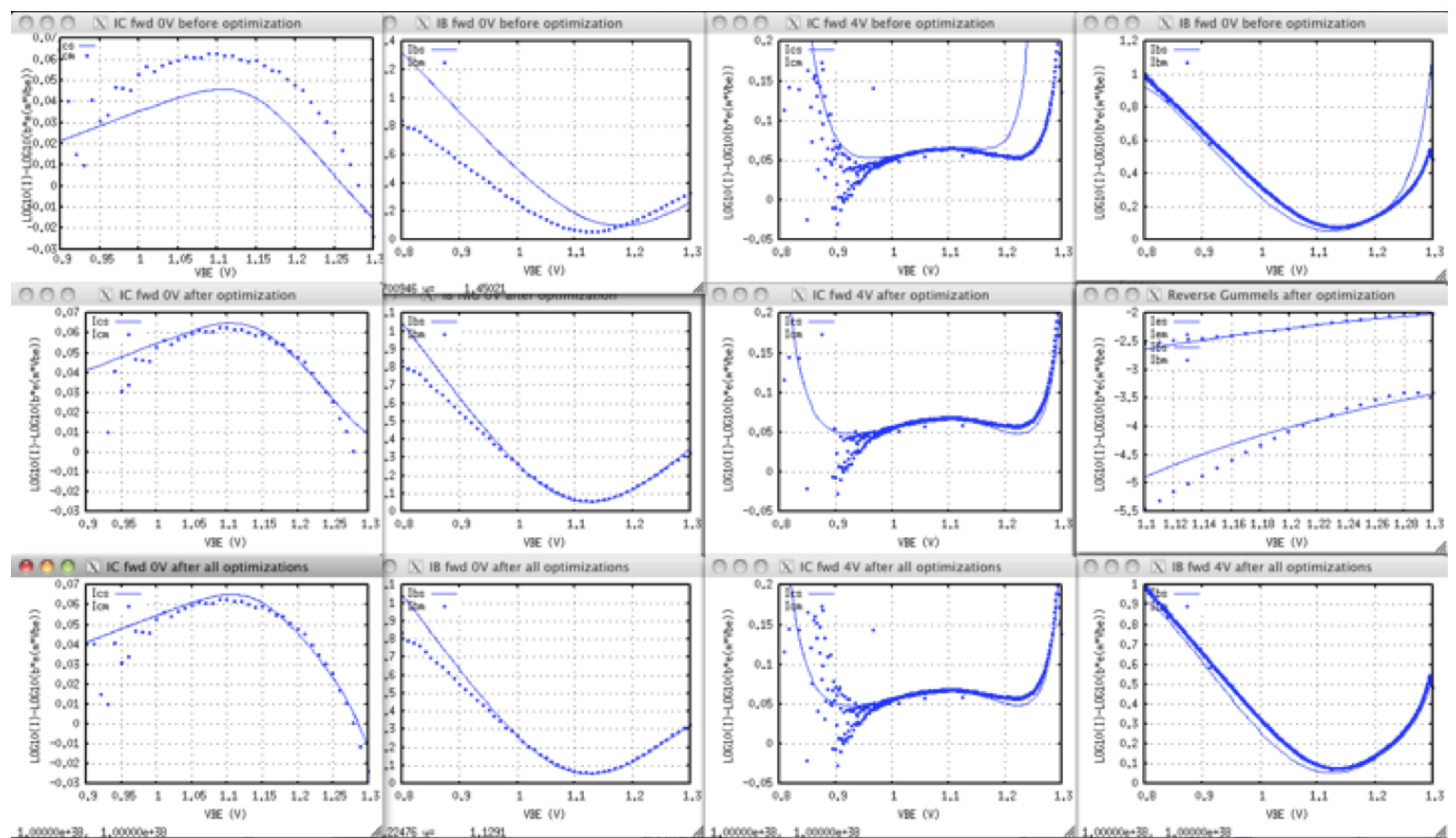


**Figure 4.1.** A snapshot of the automated process that performs the precision calibration using the data transformation. The top row shows the starting  $\delta$ s of the measured data and model for four different datasets and the bottom row shows the final  $\delta$ s after optimization of model parameter values.

Note that at this time, the output characteristic curves shown in the right hand plot of Figure 3.9 are not used in the automated process, as the data is too sparse to obtain accurate optimizations and the parameters shown there are already optimized from the reverse Gummel characteristic.

Following the completion of the reverse Gummel characteristic parameter extraction, the previous four characteristic collector and base current  $\delta$  curves for  $V_{BC}=0$  and  $V_{BC}=4$  are recalculated with the full set of extracted parameters (EA, EAIE, IBCI, IBEL, IBEN, IKF, IS, ISRR, NCI, NCN, NEI, NF, NKF, RBI, RBX) to show the analyst if the accuracy of earlier extractions have been adversely impacted by the extraction of the latter parameters. These recalculations are displayed as the third row of plots at the bottom of all the columns. In principle, the whole global process could be iterated if the recalculations indicate further accuracy could be obtained, but thus far such a case has yet to be encountered.

The plots provide the analyst with real-time information as an aid to tuning the optimizations.

In addition, in unattended batch mode the plots are stored so that analysts can later view and quickly verify that the optimization has accurately extracted the model parameters to match the calibration data. The accuracy of the process is demonstrated in Figure 4.2, which shows that the visible deviations from the transformed calibration data in the previous figure are virtually invisible in the optimized  $V_{BE}$  range when the data are plotted directly without transformation.

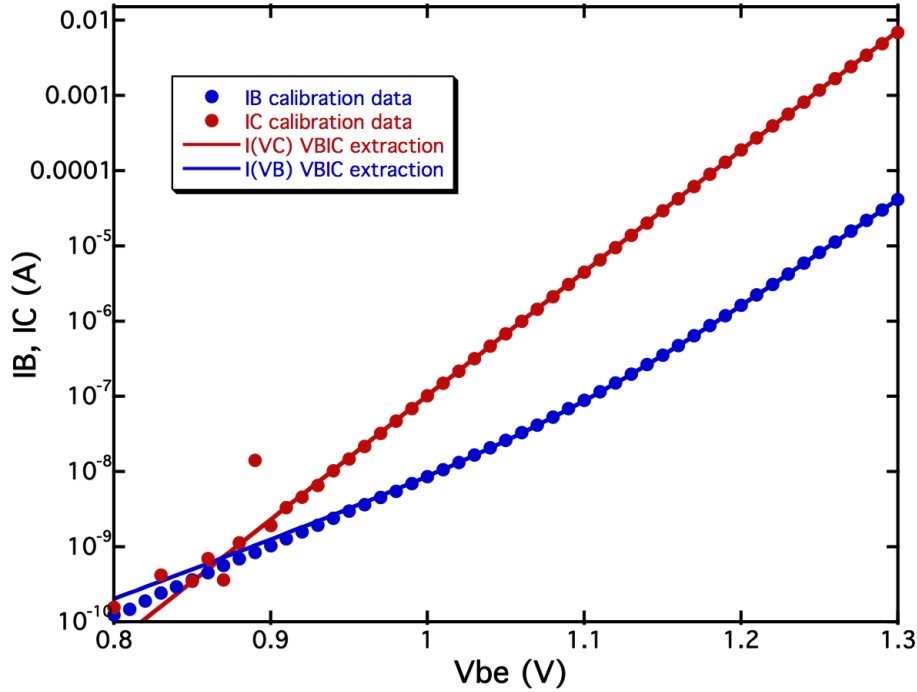


**Figure 4.2.** A plot of the  $V_{BC}=0$  collector and base currents demonstrating the high accuracy of the extracted VBIC model in matching the calibration data.

#### 4.4.1 Temperature Dependence of Final Optimization

The data and model fits shown in Figure 4.2 are for room temperature ( $25^{\circ}\text{C}$ ). For many applications, it is necessary for the model to have good temperature-dependent characteristics over a range of temperatures. It is important that the parameters optimized to match room temperature data enable sufficient precision to model device-to-device variability, yet preserve good temperature tracking behavior. To achieve this, the temperature tracking exponential parameters, XII, XIKF, XIN, XIS, XRCI, XRCX, XRE, and the thermal resistance parameter RTH presently are set for best temperature behavior for most devices. These parameters are determined by the aggregate behavior of a group of devices instead of matched to individual devices.

It would be ideal to have calibration data available over a range of temperatures so that temperature dependent device-to-device variability is accurately calibrated in these parameters. In this exercise, such data was not generally available and a limited amount of temperature dependent

data exists. This data is used as quality control data in the microfab where these transistors are manufactured and is taken at  $-40$ ,  $25$ , and  $90^\circ\text{C}$ . Figure 4.3 shows the temperature-dependent performance of the automated VBIC extraction compared to this data for  $V_{BC}=0$  collector and base currents.

The optimal fit to the data is at  $25^\circ\text{C}$  but the  $90^\circ\text{C}$  fit is very good in the  $V_{BE}$  range of interest ( $0.9$  to  $1.3$  Volts). The worst fit to the data is the collector current at low temperatures,  $-40^\circ\text{C}$ . In all cases, the fit is adequate for most modeling applications but the high precision applications of concern here demand improvement upon the low temperature case.

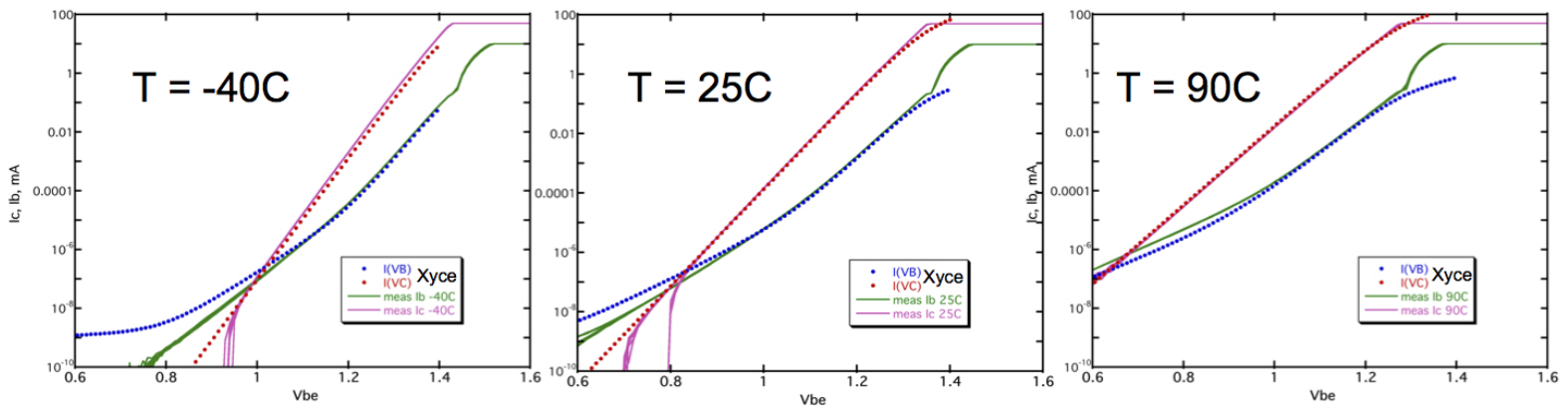


**Figure 4.3.** Plots comparing collector and base currents at  $V_{BC}=0$  to data taken from  $-40$  to  $+90^\circ\text{C}$ .



# Chapter 5

## Summary and Conclusions

High accuracy in compact model descriptions of transistor devices can be required in many different scenarios. Certain circuits [4] require highly accurate models in order for simulations of circuit operation to be useful. Other applications include using simulations to accurately quantify the differences inherent in circuits using components that have part-to-part variability. In this latter case, model descriptions of device behaviors must possess error magnitudes less than the differences in behavior between devices.

This document describes a data transformation technique which enables model calibration, error examination, and quantification of errors in model fits. The technique consists of fitting a modeling *residual* to a measured data *residual* and this method amplifies model to measurement differences. In discussions of model fit errors, error magnitudes are sometimes characterized in parts-per-million (ppm) for small errors. An error of 0.1% can be described as 1 part in a thousand or a 1000ppm. The data transformation technique has been shown to result in errors of model fits to data of as small as 10ppm.

This technique is dependent upon a particular calibration process for maximum accuracy. This present work has focused on investigating and implementing a data calibration and optimization process to fully utilize the data transformation technique. It is this process coupled with the transformation that results in low ppm errors.

Associated with this technique is a further refinement step which is not described in this report. This technique uses the highly accurate device models resulting from the present work and combining these models in a circuit where other circuit parameters are optimized to obtain key circuit characteristic matchings with low error magnitudes. In this way, the 10ppm level of errors can be extended beyond the device level to the circuit level. This method will be described in a future report.



# References

- [1] A. P. Brokaw. A Simple Three-Terminal IC Bandgap Reference. *IEEE Journal of Solid-State Circuits*, SC-9(6):388–393, Dec. 1974.
- [2] R. J. Widlar. New Developments in IC Voltage Regulators. *IEEE Journal of Solid-State Circuits*, SC-6(1):2–7, Feb. 1971.
- [3] J. S. Brugler. Silicon Transistor Biasing for Linear Collector Current Temperature Dependence. *IEEE Journal of Solid-State Circuits*, SC-2(1):57–58, Jun. 1967.
- [4] P. E. Allen. Lecture 390 - Bandgap Voltage References. *ECE 4430 - Analog Integrated Circuits and Systems*, SC-6(1):1–14, Dec. 2001.
- [5] H. Gummel and H. Poon. An integral charge control model of bipolar transistors. *Bell System Technical Journal*, 49:827–852, May-June 1970.
- [6] M. Rudolph. *Introduction to Modeling HBT's*. Artech House, Boston/London, 2006.
- [7] F. Sischka. *Gummel-Poon Bipolar Model: Model Description Parameter Extraction*. Agilent Technologies GmbH, Munich, 1990.
- [8] C. McAndrew. *Vertical Bipolar Intercompany Model Web Page*. <http://www2.fht-esslingen.de/institute/iafgp/neu/VBIC>, 1999.
- [9] E. Keiter, T. Mei, T. Russo, R. Schiek, P. Sholander, H. Thornquist, J. Verley, and D. Baur. Xyce Parallel Electronic Simulator Sandia Users Guide, Version 6.2. *Technical Report SAND2014-18007*, 2014.
- [10] B. Adams, M. Ebeida, M. Eldred, J. Jakeman, L. Swiler, J. Stephens, D. Vigil, T. Wildey, W. Bohnhoff, K. Dalbey, J. Eddy, K. Hu, L. Bauman, and P. Hough. Dakota, A Multilevel Parallel Object-Oriented Framework for Design Optimization, Parameter Estimation, Uncertainty Quantification, and Sensitivity Analysis: Version 6.1 User's Manual. *Technical Report SAND2014-4633*, 2014.



# Appendix A

## VBIC Model Parameters

**Table A.1.** VBIC Model Parameters.

Parameter	Description of Parameter	Units
<i>Parameters Describing Ideal DC Operation</i>		
Is	transport saturation current	A
Isrr	reverse transport current scaling factor	no units
Nf	forward emission coefficient	no units
Nr	reverse emission coefficient	no units
Ea	activation energy for Is	V
Dear	activation energy or Isrr	V
Xis	temperature exponent of Is	no units
Xisr	temperature exponent of Isrr	no units
Tnf	temperature coefficient of Nf	no units
Ibei	ideal BE saturation current	A
Nei	ideal BE emission coefficient	no units
Wbe	intrinsic fraction of total Ibe	no units
Eaie	activation energy for Ibei	V
Xii	temperature exponent of Ibei, Ibc <sub>i</sub> , Ibeip, Ibcip	no units
Ibc <sub>i</sub>	ideal BC saturation current	A
Nc <sub>i</sub>	ideal BC emission coefficient	no units
Eaic	activation energy for Ibc <sub>i</sub> and Ibeip	V
<i>Parameters Describing Nonideal Base Currents</i>		
Iben	BE leakage saturation current	A
Nen	BE leakage emission coefficient	no units
Ibcn	BC leakage saturation current	A
Ncn	BC leakage emission coefficient	no units
Eane	activation energy for Iben	V
Xin	temperature exponent of Iben, Ibcn, Ibenp, Ibcnp	no units

**Table A.2.** VBIC Model Parameters.

Parameter	Description of Parameter	Units
<i>Parameters of Base Charge <math>q_b</math></i>		
Vef	forward Early voltage	V
Ver	reverse Early voltage	V
Ikf	forward base high-current injection	A
Ikr	reverse base high-current injection	A
Xikf	temperature exponent of Ikf	no units
Qbm	switches $q_b$ formula	no units
Nkf	exponent for $q_b$ calculation	no units
<i>Breakdown Parameters</i>		
Ibbe	BE breakdown saturation current	A
Vbbe	BE breakdown voltage	V
Nbbe	BE breakdown emission coefficient	no units
Tvbbe1	temperature coefficient of Vbbe	no units
Tvbbe2	second temperature coefficient of Vbbe	no units
Tnbbe	temperature coefficient of Nbbe	no units
Avc1	BC weak avalanche parameter	no units
Avc2	BC weak avalanche parameter	no units
Tavc	temperature coefficient of Avc2	no units
<i>Depletion Capacitances</i>		
Fc	Forward-bias depletion capacitance limit	no units
Cje	BE zero-voltage capacitance	F
Pe	BE diffusion voltage	V
Me	BE grading coefficient	no units
Aje	BE capacitance smoothing factor	no units
Cjc	BC zero-voltage capacitance	F
Pc	BC diffusion voltage	V
Mc	BC grading coefficient	no units
Ajc	BC capacitance smoothing factor	no units
Vrt	BC capacitance reach-through voltage	V
Art	BC capacitance reach-through smoothing factor	no units

**Table A.3.** VBIC Model Parameters.

Parameter	Description of Parameter	Units
<i>Diffusion Capacitances and Transit Times</i>		
Tf	ideal forward transit time	s
Tr	ideal reverse transit time	s
Xtf	excess transit-time coefficient	no units
Vtf	excess transit-time dependency on $V_{bc}$	V
Itf	excess transit-time dependency on $I_F$	A
Qtf	excess transit-time dependency on Early effect	no units
Td	forward excess time delay	s
<i>Quasi-Saturation Model</i>		
Rci	intrinsic collector resistance	$\Omega$
Xrci	temperature exponent of Rci	V
Gamm	epitaxial collector doping parameter	
Vo	drift saturation voltage	V
Xvo	temperature exponent of Vo	no units
Href	high current RC factor	no units
Qco	quasi-saturation excess charge parameter	no units
<i>Extrinsic Resistances and Capacitances</i>		
Rcx	extrinsic collector resistance	$\Omega$
Rbx	extrinsic base resistance	$\Omega$
Rbi	intrinsic base resistance	$\Omega$
Re	extrinsic emitter resistance	$\Omega$
Xrcx	temperature exponent of Rcx	no units
Xrbx	temperature exponent of Rbx	no units
Xrbi	temperature exponent of Rbi	no units
Xre	temperature exponent of Re	no units
Cbeo	extrinsic BE capacitance	F
Cbco	extrinsic BC capacitance	F

**Table A.4.** VBIC Model Parameters.

Parameter	Description of Parameter	Units
	<i>Substrate Transistor Parameters</i>	
Isp	substrate transport saturation current	A
Nfp	substrate forward emission coefficient	no units
Eap	activation energy for Isp	V
Ibeip	ideal substrate BE saturation current	A
Ibenp	non ideal substrate BE saturation current	A
Ibcip	ideal substrate BC saturation current	A
Ncip	ideal substrate BC emission coefficient	no units
Eais	activation energy for Ibcip	V
Eanc	activation energy for Ibcnp and Ibenp	V
Ibcnp	nonideal substrate BC saturation current	A
Ncnp	nonideal substrate BC emission coefficient	
Wsp	fraction of substrate transfer current depending on $V_{bep}$	no units
Eans	activation energy for Ibcnp	V
Ikp	substrate forward base high-current injection	A
Cjcp	SC zero-voltage capacitance	F
Cjep	substrate BC zero-voltage capacitance	F
Ps	SC diffusion voltage	V
Ms	SC grading coefficient	no units
Ajs	SC capacitance smoothing factor	no units
Rs	substrate resistance	$\Omega$
Rbp	substrate base resistance	$\Omega$
Xrs	temperature exponent of Rs	no units
Xrbp	temperature exponent of Rbp	no units
	<i>1/f noise</i>	
Kfn	BE flicker (1/f) noise coefficient	no units
Afn	BE flicker (1/f) noise exponent	no units
Bfn	BE flicker (1/f) noise dependence	no units
	<i>Temperature Parameters</i>	
Tnom	ambient temperature at parameter extraction	$^{\circ}\text{C}$
Dtemp	actual ambient temperature (actually delta from set temp)	$^{\circ}\text{C}$
Rth	thermal resistance	K/W
Cth	thermal capacitance	J/K





**Sandia National Laboratories**